Delayed lubricant depletion of Slippery Liquid Infused Porous Surfaces using precision nanostructures

Sophia K. Laney,[1‡] Martyna Michalska,[1‡] Tao Li,[1‡] Francisco V. Ramirez,[1] Mark Portnoi,[1] Junho Oh,[2,3] Iain G. Thayne,[4] Ivan P. Parkin,[5] Manish K. Tiwari,[2,6] and Ioannis Papakonstantinou[1*]*

[1] *Photonic Innovations Lab, Department of Electronic & Electrical Engineering, University College London, Torrington Place, London WC1E 7JE, UK*

[2] *Nanoengineered Systems Laboratory, Department of Mechanical Engineering, University College London, Torrington Place, London WC1E 7JE, UK*

[3] *Department of Mechanical Engineering, Hanyang University, Ansan, 15588. South Korea*

[4] *James Watt School of Engineering, University of Glasgow, Glasgow G12 8LT*

[5] *Department of Chemistry, University College London, Torrington Place, London WC1E 7JE, UK*

[6] *Wellcome/EPSRC Centre for Interventional and Surgical Sciences (WEISS), University College London, London, W1W 7TS, UK*

[‡] *These authors contributed equally*

[*]*Email: i.papakonstantinou@ucl.ac.uk; m.tiwari@ucl.ac.uk*

ABSTRACT: Slippery Liquid Infused Porous Surfaces (SLIPS) are an important class of repellent materials, comprising micro/nano-textures infused with a lubricating liquid. Unlike superhydrophobic surfaces, SLIPS do not rely on a stable air-liquid interface and thus can better manage low surface tension fluids, are less susceptible to damage under physical stress, and are able to self-heal. However, these collective properties are only efficient as long as the lubricant remains infused, which has proved challenging. We hypothesized that, in comparison to a nanohole and nanopillar morphology, the 'hybrid' morphology of a hole within a nanopillar, namely a nanotube, would be able to retain and redistribute lubricant more effectively; owing to capillary forces trapping a reservoir of lubricant within the tube, whilst lubricant between tubes can facilitate redistribution to depleted areas. By virtue of recent fabrication advances in Spacer Defined Intrinsic Multiple Patterning (SDIMP), we fabricated an array of silicon nanotubes, and equivalent arrays of nanoholes, and nanopillars (pitch; 560 nm, height; 2 µm). After infusing the nanostructures (pre-rendered hydrophobic) with lubricant Krytox 1525, we probed the lubricant stability under dynamic conditions and correlated the degree of the lubricant film discontinuity to changes in the contact angle hysteresis. As a proof-of-concept, the durability test, which involved consecutive deposition of droplets onto the surface amounting to 0.5 liters, revealed a 2-fold and 1.5-fold enhancement of lubricant retention in nanotubes, in comparison to nanopillars and nanoholes respectively; showing a clear trajectory for prolonging the lifetime of a slippery surface.

INTRODUCTION

Liquid repellent surfaces have been an active area of research for some decades, with a predominant focus on superhydrophobic lotus inspired-structures[1–4]. An upsurge of interest in pitcher plant-inspired surfaces, known as Slippery Liquid Infused Porous Surfaces (SLIPS), has been observed ever since their introduction in 2011.[5] This family of non-wettable surfaces

which comprise a thin lubricating layer trapped within surface roughness, resides at the forefront of the literature, having consistently been shown to succeed where their gas-cushioned counterparts fail; in repelling organic liquids or complex mixtures with low surface tension, sustaining no damage under physical stress, and an ability to self-heal.[6,7] Prized for their anti-adhesive nature, SLIPS bestow interfacial properties that are highly desired across a broad range of applications including anti-icing,[8,9] drag-reducing properties,[10] heat transfer,[11] anti-fouling coatings in the marine[12] and medical sectors,[13,14] non-stick packaging,[15] and droplet manipulation.[16]

To achieve liquid repellence, SLIPS essentially exploit the immiscibility of lubricants with other liquids. A low surface energy lubricant is infused into the surface structure, and the lubricant forms the interface with the immiscible working liquids (e.g., water, ethanol), as opposed to the solid surface, thus resulting in very low contact angle hysteresis (minimal adhesion). In order to attain these properties, three criteria need to be met: (i) the solid substrate must have a higher affinity for the lubricant over the droplet, (ii) the lubricant and the working fluid must be immiscible, (iii) the lubricant must wick into, spread and stably adhere within the structure.[5,17] The prime source of failure for SLIPS lies in this third criterion and the poor ability of the structure to retain the lubricant leading to drainage of the lubricant layer causing contact line pining of the working fluid on the exposed solid structures.[18,19] Exploiting the physical interaction between the lubricant and the structure is, therefore, crucial for its retention.

In this regard, recent fabrication capabilities, propelled in part by the design and manufacture of superhydrophobic surfaces, have given rise to an expansive array of possible nano- and micro-architectures.[4,20] Nonetheless, efforts to design a structure capable of enhanced lubricant retention are still on-going, with the effect of geometric surface parameters on lubricant retention under flow highlighted as an area requiring further work.[21] Maximizing the capillary forces, which hold the lubricant within the structure against the action of gravity and shear

force, is clearly an important consideration. Such capillary forces are only generated when the sizes of the features are smaller than the capillary length of the lubricating liquid.[22] Whilst micro-roughness typically satisfies this criterion, under high shear conditions the effective capillary length of the lubricant reduces to micron length scales (~ μm), thereby permitting lubricant depletion, and exposing the underlying microstructures.[23] Conversely for nanostructures, the lubricant layer remains stable until the thickness reduces to a size comparable to the feature height.[24] Additionally, the capillary pressure which retains the lubricant is much greater for nanostructures, owing to the inverse relationship with the spacing between structural domains (nanointerstices).[25] Of course, all nanostructured surfaces do not perform equally, and further probing of nanostructure features has elucidated the benefits of a closed-cell system (*i.e.* nanoholes/pores),[24] as opposed to an open-cell system (interconnected networks *i.e.* nanopillars).[26] Here, the isolated domains of lubricant act as a physical barrier to depletion,[19] however paradoxically, this retention can prevent replenishment and self-healing. As the lubricant layer thins, a surface with a lower solid fraction (minimized flat areas where capillary forces cannot act) can benefit SLIPS performance, owing to fewer sites for water contact line pinning.[27] Intermolecular forces can also be maximized through increasing the surface area (roughness) of the nanostructures.[23] Based on these considerations, it is necessary to generate a nanostructure which has a low solid fraction, a high roughness, and the ability to simultaneously retain and replenish lubricant. One well-studied example which satisfies these criteria is an inverse colloidal monolayer, where structural dimensions and corresponding roughness are determined by the nanoparticle size.[24] Another such structure is a hybrid between a nanopillar (NP) and a nanohole (NH); namely, a nanotube (NT), where enhanced tunability stems from decoupling the individual nano-feature dimensions (height, spacing, wall thickness). Recent advances in atomic layer deposition-assisted processes, such as Spacer

Defined Intrinsic Multiple Patterning (SDIMP),[28] have enabled the controlled fabrication of such nanotube structures; creating an opportunity for further studies.

For the first time, we fabricate and functionalize a silicon nanotube sample and compare its ability to retain lubricant (Krytox 1525 – fluorinated oil immiscible with most working fluids)[29] with nanohole and nanopillar samples of equivalent dimensions, under dynamic conditions with water as the working fluid. To test the stability of the lubricant within each structure, we perform two different tests and correlate the degree of the lubricant film discontinuity to changes in the contact angle hysteresis (CAH). Firstly, we performed a shear tolerance test which revealed all nanostructures were able to retain the lubricant through capillary action up to the tested 10k rpm; yielding no significant changes in CAH. Secondly, we designed and performed a harsher droplet shedding test, with consecutive deposition of small droplets at moderate rates (~16 µl, 2 drops/s; known to challenge the lubricant retention, as opposed to larger volumes or continuous flow and higher rates)[29] onto the tilted surface amounting to 0.5 liters. We observe a 2-fold and 1.5-fold enhancement of lubricant retention in nanotubes, in comparison to nanopillars and nanoholes, respectively.

EXPERIMENTAL METHODS

Nanostructure fabrication. The nanostructures of hole, pillar and tube morphologies were fabricated according to a previously reported method.[28] Briefly, a Si wafer (MicroChemicals) with a deposited SiO_2 layer of 200 nm thickness was coated with a primer (TI Prime, MicroChemicals), and subsequently a photoresist (PR) layer (ma-N 405, Microresist technology). Laser Interference Lithography (LIL) was employed to pattern the PR with square-packed holes or pillars. The residual PR layer was then removed via oxygen etching to expose the underlying SiO_2 layer. Reactive Ion Etching (RIE) was performed to etch the SiO_2 hard mask using CHF_3/Ar plasma at a temperature of 20°C (PlasmaPro NGP80 RIE, Oxford

instruments). The pattern was transferred into the underlying Si via RIE using Cl_2 plasma (ASE, STS MESC Multiplex ICP). Etching was performed until mask consumption to generate nanohole or nanopillar arrays. Fabrication of the nanotube arrays was performed via SDIMP.[28] Specifically, an Al_2O_3 spacer layer was applied to a Si nanohole array via Atomic Layer Deposition (ALD). RIE under Cl_2 plasma was conducted until the point of Al_2O_3 consumption to yield Si nanotubes. Detailed etching conditions for all RIE processes are listed Tables S1-S3.

Nanostructure characterization. Scanning Electron Microscopy (SEM) was performed using a Field Emission Zeiss Ultra Plus scanning electron microscope with a Gemini column operating at an accelerating voltage of 2-20 kV. ImageJ (https://imagej.nih.gov/ij/) was used for statistical analysis of the nanostructure dimensions such as pitch, height, diameters.

Surface functionalization. The samples were immersed in 1H,1H,2H,2H-Perfluorodecyltrimethoxysilane (PFDTES) in anhydrous toluene (2% v/v) at room temperature for 24 h, and subsequently annealed at 120°C for 30 min.

Lubricant infiltration. An excess of lubricant was poured atop the surfaces which were then placed in a low-pressure vacuum chamber (pressure ~0.001 atm) for 1 h. To remove the excess lubricant, the surfaces were tilted at 70° under ambient conditions for 24 h, with an absorbent cloth placed underneath.

Contact angle measurements. Both advancing and receding contact angles were measured using a custom designed goniometry setup. The setup consists of a syringe pump (Cole-Parmer Single-syringe infusion pump), a needle (BD PrecisionGlide™ needles, 18G), and an imaging device (Thorlab, model DCC1240). Droplets of approximately 20 µl were deposited onto the surfaces and further extracted using the syringe pump to measure the advancing and receding contact angle, respectively. The videos taken during droplet deposition and extraction were

processed through a Matlab script for contact angle measurements,[30] which is available from the corresponding author upon reasonable request.

The shear tolerance test. The samples, 2 x 2 cm^2, were prepared with an initial excess of lubricant on the surface and affixed onto individual glass microscope slides, 2.5 cm from the center of the slide, with a piece of flat silicon affixed at the opposite end to ensure balancing of the slide. The slide containing the sample was then placed onto the spin coater (SCS G3 Spin Coater). The samples were subjected to increasing spin speeds from 1k to 10k rpm for 60 s at a ramping rate of 3.2. The contact angle hysteresis (CAH) was measured after each spinning cycle (three repeat measurements) and was used to indicate the loss of lubricant from the structure.

Droplet shedding test. Samples were placed on a 45°-tilted stage with needles placed 1 cm from the sample, connected via tubing to a water reservoir and automatic pump (see Figure 3a for schematic). Droplet volume (16 µl) was measured by weighing a known number of water droplets (repeated three times) and using the density of water. The water flow (2 droplets/s) was chosen to be slow enough to ensure single droplets landed on the surface rather than a constant stream, but fast enough so that all points could be collected in one day to avoid effects ranging from self-healing to evaporation. Figure 3a illustrates the setup and shows the five locations on the sample where CAH measurements were taken. Only one point was taken on the left and right of the sample as these areas were not in the pathway of the droplet, however tests were performed to ensure there was no difference across the left side (top, middle and bottom) and right side (top, middle and bottom).

Weighing experiment. Samples were weighed before infiltration. The next weight measurement was taken after infiltration and drainage of excess lubricant. Subsequently, measurements were taken after dropwise deposition (according to the protocol in the droplet

shedding test) of 150, 250, 350, and 500 ml water. Weights of the three samples were normalized to the surface area, and to the corresponding 'dry' weight.

RESULTS AND DISCUSSION

To systematically probe the lubricant retention capabilities of the three nanostructures, we employ a nanotube array originating from a previous investigation, focused on its excellent antireflective properties.[28] We fabricated corresponding arrays of nanoholes and nanopillars with equivalent pitch (560 nm), heights (~2 μm), and top diameters (~300 nm), as listed in Table 1. The nanotube dimensions, with comparable intra- and inter-tube spacing, allow for both lubricant retention and redistribution, whilst the high surface roughness provided by an AR~7 increases the inherent resistance to shear. Laser interference lithography, plasma etching and for the nanotubes, subsequent ALD-assisted processing (SDIMP)[28] were employed to generate the nanostructure arrays as seen in Figure 1a-c. Here, SDIMP allows for freedom in the nanotube design, whereby the inter- and intra-tube spacing can be realized with ALD precision.

As discussed, the water repellence of a SLIPS is attributed to the water-immiscible lubricant film held within and above the surface of a porous structure, yet, characteristics of the underlying porous structure play an important role in the droplet mobility, redistribution characteristics, and capillary retention.[25] As the lubricant film begins to deplete, the mobility of a droplet (sliding speed) is known to be reduced on a surface with a larger solid fraction $\emptyset_S$; the fraction of the solid that is exposed to the working fluid (water in this example). Characterization of the three nanostructures revealed a $\emptyset_S$ of 0.1 for nanotubes, 0.7 for nanoholes and 0.2 for nanopillars, providing initial indications that droplet mobility may be most hindered on the nanoholes. In terms of lubricant redistribution, broadly speaking, structures able to hold a greater volume of lubricant per unit area (nanotubes > nanopillars >

nanoholes; Table 1) benefit from the increased capacity to redistribute and replenish depleted areas (provided the lubricant is not isolated, as is the case for the nanoholes). It is also known that surfaces possessing a greater degree of roughness *R* (calculated total surface area of the structure over the projected area), are able to entrap oil more effectively through a combination of capillary and van der Waals forces.[23] Indeed, there is a critical roughness value (R_{crit}) which needs to be exceeded in order for a lubricant film to be thermodynamically stable.[24] For the case of a water droplet as the working fluid and Krytox 1525 as the lubricant, $R_{crit} > 1.2$ (Text S1). All surfaces exceed this threshold (Table 1) indicating that without external perturbances, the lubricant would be stably adhered within all nano-structured surfaces.

To further quantify the effect of structure theoretically, we determined the difference in energy between two possible configurations, as previously described:[5] (1) the structure is fully wet by water (E_W) and (2) the structure is fully wet by lubricant in the presence (E_{LW}) or absence (E_L) of water. To ensure the structure is preferentially wet by the lubricant as opposed to water, $\Delta E_{LW} = E_W - E_{LW} > 0$, and $\Delta E_L = E_W - E_L > 0$. Derivations of these equations can be found in Text S2. Values are shown in Table 1 and indicate that all structures far exceed the criteria but moreover the tubes are shown theoretically to be most stable.

Table 1. Dimensions of the nanostructures of the same pitch (560 nm) and calculated values for the roughness *R*, solid fraction $\emptyset_S$, capacity for lubricant per cm^2 *V*, the difference in energy when the structure is fully wet by the lubricant in the presence ΔE_{LW} or absence of water ΔE_L.

Morphology	**Height / nm**	**Diameter / nm**	R	$\emptyset_S$	V **/ ml**	ΔE_{LW}	ΔE_L
Nanotubes	1994 ± 28	Inner: 238 ± 9 Outer: 311 ± 10	11.9	0.10	1.8 x 10^{-4}	*515*	*618*
Nanoholes	1771 ± 36	348 ± 13	7.2	0.70	5.4 x 10^{-5}	*291*	*394*
Nanopillars	1857 ± 30	292 ± 12	6.4	0.21	1.5 x 10^{-4}	*254*	*357*

For the SLIPS preparation, all samples were treated similarly, and were first rendered hydrophobic through functionalization with a silane (PFDTES), as depicted schematically in Figure 1d and detailed in the experimental section. The apparent advancing (θ^a_{adv}) and receding (θ^a_{rec}) water contact angles and the CAH served as indicators of the successful modification from hydrophilic (θ^a_{adv}<10°) to hydrophobic upon silane-functionalization, resulting in $\theta^a_{adv,Tube}$=155°±1, $\theta^a_{adv,Hole}$=145°±2, and $\theta^a_{adv,Pillar}$=148°±2 with CAH of 30°±2, 145°±2 and 18°±2, respectively (Figure 2a,b). After immersion of the surfaces in the lubricant, with infiltration into the structure encouraged by the hydrophobic coating as well as vacuum degassing, excess lubricant was removed through means of wicking onto an absorbent cloth over a period of 24 h. Measurement of the advancing contact angle revealed equivalent wetting behavior across the sample set with $\theta^a_{adv,Tube,Hole,Pillar} \approx 120°$ and CAH < 3° (Figure 2a,b). The lubricant is observed to form a wetting ridge (lubricant meniscus surrounding the droplet; Figure 3b) and based on the interfacial tensions of the lubricant-water pair, cloaking of the droplet by the lubricant is expected (see Text S3).

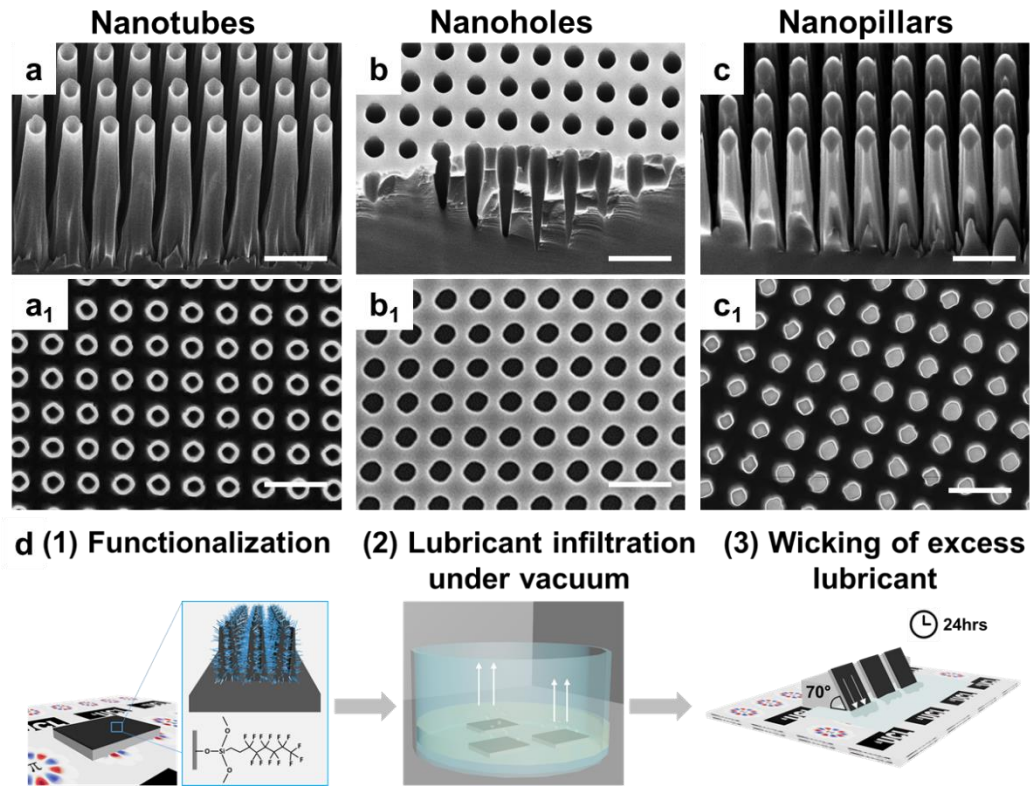

Figure 1. (a-c) Side view and, (a_1-c_1) top view SEM images of the nanotube, nanohole, and nanopillar structures, respectively. Scale bars = 1 µm. (d) Schematic of the SLIPS samples preparation flow: (1) functionalization with PFDTES; (2) infusion of the lubricant into the nanostructures by submersion and subsequent degassing under vacuum; (3) wicking of excess lubricant by tilting the samples at an angle of 70° atop of an absorbent cloth for a duration of at least 24 h.

One of the tests frequently performed to assess the durability of a slippery surface, namely a shear tolerance test, involves subjecting the surfaces to increasing centrifugal forces (spin speeds) and comparing the resultant water CAH (Figure 2c). After being subjected to a speed of 1k rpm for 1 min, the CAH remained below 5° indicating a continuous lubricant film was still present. Increasing the speed further up to 10k rpm also revealed no significant increase in the CAH for each of the surfaces; consistent with previous studies on nanostructured surfaces.[24] Under these conditions capillary forces are responsible for trapping the lubricant film, and

remain effective so long as the capillary length k^{-1} of the lubricant remains greater than the length scale of the nanostructures ($k^{-1} = \sqrt{\frac{\gamma}{\rho g}}$ where γ is the surface tension, and ρ is the density of the fluid, and g the gravitational acceleration). In the absence of spinning, the capillary length of Krytox 1525 is ~1 mm. However, as the spin rate increases, the capillary length decreases and ultimately reaches a value of ~tens μm at 10k rpm; thus, the lubricant remains trapped within a nanostructured surface, as previously reported.[23]

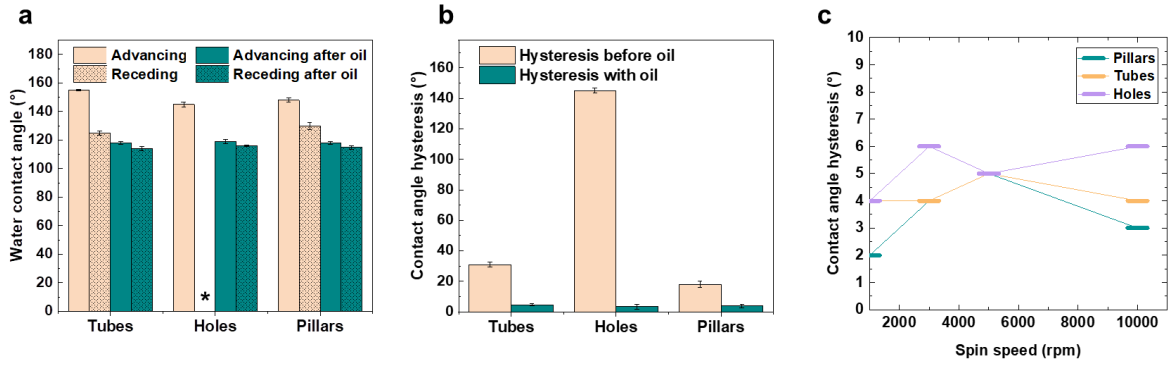

Figure 2. (a) Advancing and receding water contact angles on the three different structured silanized surfaces before (orange) and after (green) lubricant infiltration indicating the higher advancing contact angles on the silanized surfaces without lubricant (the asterisk indicates pinning) and the reduced contact angles that are consistent across the three, after lubricant infiltration. (b) Water contact angle hysteresis of the three structured silanized surfaces before and after lubricant infiltration. After lubricant infiltration, all three surfaces display very low CAH (< 5°). (c) Water contact angle hysteresis on the three different lubricated nanostructured samples after the shear tolerance test. The spin rate starts at 1k rpm and increases to 10k rpm for a time of 60s at each speed.

Although capillary forces are able to hold the lubricant within the structure whilst being subjected to high shear forces, the conditions that a SLIPS would experience when deployed

are typically much harsher. Even the seemingly simple motion of a droplet being shed from a slippery surface invokes a complex interplay of surface tensions within a four-phase system. Therefore, we designed a system whereby small droplets (16 µl) were deposited from a height of 1 cm onto the surfaces, which were tilted at 45°. A small droplet volume and moderate rate of deposition (2 droplets/s) were chosen to challenge the surfaces' ability to retain lubricant; with droplets of greater volume, or continuous streams suppressing lubricant depletion by minimizing the formation of a lubricant cloaking layer and large wetting ridge, and similarly increasing the deposition rate is another known strategy for reducing wetting ridge formation. Contact angle hysteresis was measured at different intervals, across 5 different locations of the sample: left, middle top (where the droplet is deposited), center (where the drop slides), middle bottom and right. A schematic of the experimental setup and location of the measured points is shown in Figure 3a. The results are plotted in Figure 3c as contour maps, where the *x*- and *y*-axes indicate the location on the sample, and the *z*-axis contains information on the CAH.

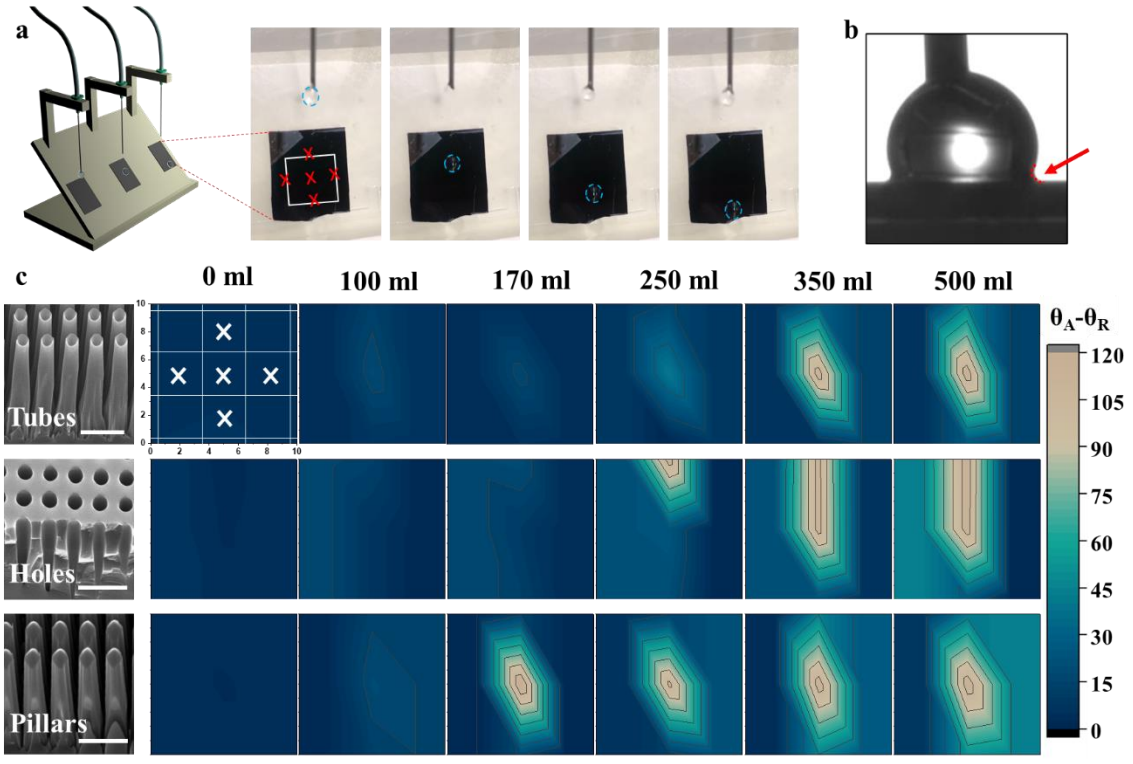

Figure 3. (a) Schematic representation of the experimental setup for the droplet shedding tests; whereby needles deposited water droplets onto the surface. A corresponding photograph highlights the locations where measurements of CAH were taken (marked with a red cross). Later photographs show the progression of a droplet as it leaves the needle, lands on the surface and slides down. (b) Photograph of a water droplet deposited onto a lubricant infused surface, with formation of a wetting ridge (outlined in red). (c) Results from the droplet shedding test. Contour maps represent the change in CAH across each surface, with the x- and y-axes mapping the location of the measurement on the sample (as shown in the above photograph), and the z-axis represents the CAH. The CAH was measured after a known volume of water had been deposited, up to 0.5 litres. Scale bars = 1 μm.

From the test, three key observations were made: (i) drainage from the nanopillars occurred first and at the center point; (ii) drainage from nanoholes occurred next but at the point of droplet deposition; (iii) drainage from the nanotubes occurred last and at the center point. Considering the morphologies, the open structure of nanopillars allows for free redistribution of the lubricant, resulting in recovery until drainage becomes significant. At which stage, pinning and depinning of the water contact line on the exposed nanostructure slows the traversing droplet, resulting in coalescence of the successive droplet at the center point (see CAH increase). This serves to amplify lubricant depletion at this location due the increasing wetting ridge; which, owing to its negative curvature and thus Laplace pressure, draws in more lubricant over time.[18,31] Following coalescence, the now larger droplet gains velocity and slides off the surface, removing lubricant as it does so.

For nanoholes, pinning is observed at the point of droplet deposition after 250 ml and continues to deteriorate in line with droplet propagation. Within the hole, capillary forces are much greater than the surface tension force pulling up the wetting ridge hence the lubricant is

retained, however the thin layer of lubricant covering the large solid fraction is easily displaced by the shearing motion and the capillary suction force exerted by a deposited or sliding droplet.[32] Moreover, the absence of an interconnected structure prevents recovery; thus, degradation occurs first where the droplet is deposited. The droplet is observed to remain at the deposition location until a successive droplet drops down and coalesces to it.

The nanotubes, having elements of both nanopillars and nanoholes, displays the best lubricant retention, and does not exhibit pinning until 350 ml has been deposited, with the location of the pinning site equivalent to the nanopillars. A combination of factors may contribute to the longevity of the lubricant layer; firstly the open structure which aids the redistribution of lubricant to depleted areas, secondly the reservoir within the tube which is retained through capillary action, thirdly the low solid fraction which renders the surface the least hindering in terms of droplet mobility, and finally, the larger volume of lubricant held per unit area compared to nanopillars (20% more) and nanoholes (230% more), also facilitating redistribution.

As an additional layer to our experiment, we weighed the three samples before lubricant infiltration, after lubricant infiltration and at regular intervals of water deposition, with weights normalized to the dry weight (no lubricant) of surfaces of equivalent area (Figure 4). Upon infiltration, the weight of the three surfaces increased by ~2.5%. Infiltration of lubricant into the structure alone would account only for an increase in weight of ~0.3%, thus indicating a lubricant film of ~18 μm is present. Water was deposited on the surfaces in the same manner as the test presented in Figure 3. The largest decrease in weight for all three nanostructured surfaces was observed after the first 150 ml of water was passed over the surface; attributed to the easy removal of the loosely held lubricant film above the structures. Nonetheless differences between structures were observed after 150 ml, consistent with the CAH

measurements in Figure 3c; whereby nanopillars are seen to deteriorate fastest, with the lubricant film being removed to expose the nanostructures at a location in the pathway of the droplet. The nanohole and nanotube surfaces exhibit similar decreases in the weight after deposition of 150 and 250 ml of water, however after 350 ml, the weight of the nanohole surface is seen to rapidly decrease and subsequently plateau (similarly to the nanopillars); signaling that the lubricant in the pathway of the droplet has been removed. The nanotube surface on the other hand exhibits a more gradual decrease in the weight, and does not decrease to the same level as that of the nanohole or nanopillar surface after 500 ml.

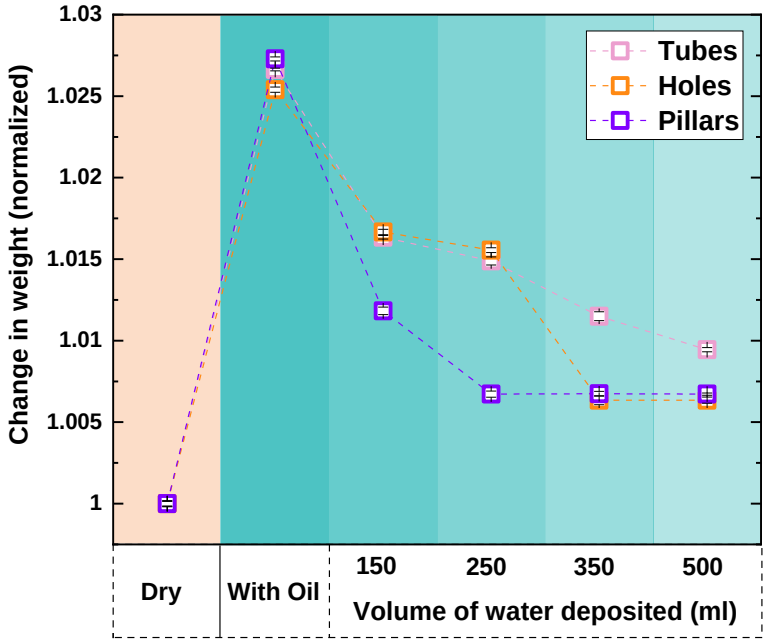

Figure 4. The observed change in weight of the three nanostructured samples after lubricant infiltration and subsequent water deposition, normalized to the dry weight (prior to lubricant infiltration). Water droplets were deposited in the same manner as shown in Figure 3a.

CONCLUSION.

In summary, we present proof-of-concept experiments which demonstrate how by simply tuning the morphology of the nanostructure, the lifetime of a slippery surface can be extended.

The fabricated nanotube sample displayed a 2-fold enhancement in lubricant retention in comparison to nanopillars when subjected to a harsh droplet shedding test. A likely explanation being that, as the lubricant layer thinned, the low solid fraction of the nanotubes enabled greater droplet mobility; decreasing the time the droplet spent on the surface and thus reducing the volume of lubricant entrained within the wetting ridge.[18] Furthermore, the capillary forces holding the lubricant within the tube prevented shear-driven lubricant removal from these areas, meanwhile lubricant outside of the tube facilitated redistribution to depleted areas (deposition location). Whilst we have focused solely on the role of the nanostructure in lubricant retention, the choice of the lubricant itself can also enhance the lifetime; with lubricants of higher viscosities having been shown to impede drainage,[33] and non-cloaking lubricant-working fluid combinations preventing additional lubricant removal with each shed droplet.[34] Overall, with modern-day fabrication capabilities (e.g. SDIMP) providing vast freedom in nanostructure design, we envision that further optimization in the nanotube fabrication (concentric or quadruple nanotubes, lowering of the pitch) can elicit even greater lubricant retention, and our preliminary results will help to pave the way to achieve durable SLIPS surfaces. Furthermore, as previously demonstrated SDIMP-generated structures can be successfully imprinted into polymer films, enabling large-scale production and wide applicability.

ASSOCIATED CONTENT

Supporting Information. The manuscript is accompanied by (i) Supporting Tables which elaborate on; the nanofabrication conditions and times of the nanotube, nanohole and nanopillar surfaces; interfacial energy values for the lubricant and water. (ii) Supporting Text referring to; (Text S1) the critical roughness to support a stable SLIPS surface; (Text S2) the

thermodynamic stability of the lubricant film within each nanostructure; (Text S3) Spreading coefficient of the lubricant on water.

AUTHOR INFORMATION

Corresponding Author

Ioannis Papakonstantinou – Photonic Innovations Lab, Department of Electronic & Electrical Engineering, University College London, Torrington Place, London WC1E 7JE, UK;

Manish K. Tiwari – Nanoengineered Systems Laboratory, Department of Mechanical Engineering, University College London, Torrington Place, London WC1E 7JE, UK; Wellcome/EPSRC Centre for Interventional and Surgical Sciences (WEISS), University College London, London, W1W 7TS, UK

Email: i.papakonstantinou@ucl.ac.uk; m.tiwari@ucl.ac.uk

Authors

Sophia K. Laney – Photonic Innovations Lab, Department of Electronic & Electrical Engineering, University College London, Torrington Place, London WC1E 7JE, UK

Martyna Michalska – Photonic Innovations Lab, Department of Electronic & Electrical Engineering, University College London, Torrington Place, London WC1E 7JE, UK

Tao Li – Photonic Innovations Lab, Department of Electronic & Electrical Engineering, University College London, Torrington Place, London WC1E 7JE, UK

Junho Oh – Nanoengineered Systems Laboratory, Department of Mechanical Engineering, University College London, Torrington Place, London WC1E 7JE, UK; Department of Mechanical Engineering, Hanyang University, Ansan, 15588. South Korea

Francisco V. Ramirez – Photonic Innovations Lab, Department of Electronic & Electrical Engineering, University College London, Torrington Place, London WC1E 7JE, UK

Mark Portnoi – Photonic Innovations Lab, Department of Electronic & Electrical Engineering, University College London, Torrington Place, London WC1E 7JE, UK

Iain G. Thayne – James Watt School of Engineering, University of Glasgow, Glasgow G12 8LT

Ivan P. Parkin – Department of Chemistry, University College London, Torrington Place, London WC1E 7JE, UK

Notes

The authors declare no competing financial interest.

Author Contributions

S.K.L and M.M wrote the paper with support from I.P. and M.K.T.. All authors contributed to the discussion and revision of the manuscript.

† These authors contributed equally.

ACKNOWLEDGMENTS

The work was conducted in the framework of the European Research Council (ERC) starting grant IntelGlazing, grant no: 679891. We are grateful to Lloyd's Register Foundation for an International Consortium of Nanotechnology (ICON) research grant and UCL BEAMS School for a PhD studentship. Funding by the ERC grant NICEDROPS, grant no: 714712 and MKT's Royal Society Wolfson Fellowship is also gratefully acknowledged. Finally, we acknowledge the assistance of the technical team in the London Centre for Nanotechnology (LCN).

ABBREVIATIONS

SLIPS, Slippery Liquid Infused Porous Surfaces; SDIMP, Spacer Defined Intrinsic Multiple Patterning; CAH, Contact Angle Hysteresis; PR, Photoresist; LIL, Laser Interference Lithography; RIE, Reactive Ion Etching; ALD, Atomic Layer Deposition; SEM, Scanning Electron Microscopy.

REFERENCES

(1) Sun, T.; Feng, L.; Gao, X.; Jiang, L. Bioinspired Surfaces with Special Wettability. *Acc. Chem. Res.* **2005**, *38* (8), 644–652.
(2) Blossey, R. Self-Cleaning Surfaces - Virtual Realities. *Nat. Mater.* **2003**, *2* (5), 301–306.
(3) Lafuma, A.; Quéré, D. Superhydrophobic States. *Nat. Mater.* **2003**, *2* (7), 457–460.
(4) Lecointre, P.; Laney, S.; Michalska, M.; Li, T.; Tanguy, A.; Papakonstantinou, I.; Quéré, D. Unique and Universal Dew-Repellency of Nanocones. *Nat. Commun.* **2021**, *12* (1), 3458.
(5) Wong, T.-S. S.; Kang, S. H.; Tang, S. K. Y. Y.; Smythe, E. J.; Hatton, B. D.; Grinthal, A.; Aizenberg, J. Bioinspired Self-Repairing Slippery Surfaces with Pressure-Stable Omniphobicity. *Nature* **2011**, *477* (7365), 443–447.
(6) Papadopoulos, P.; Mammen, L.; Deng, X.; Vollmer, D.; Butt, H. J. How Superhydrophobicity Breaks Down. *Proc. Natl. Acad. Sci. U. S. A.* **2013**, *110* (9), 3254–3258.
(7) Lv, P.; Xue, Y.; Shi, Y.; Lin, H.; Duan, H. Metastable States and Wetting Transition of Submerged Superhydrophobic Structures. *Phys. Rev. Lett.* **2014**, *112* (19).
(8) Prakash, C. G. J.; Prasanth, R. Recent Trends in Fabrication of Nepenthes Inspired SLIPs: Design Strategies for Self-Healing Efficient Anti-Icing Surfaces. *Surfaces and Interfaces* **2020**, *21* (September), 100678.
(9) Kreder, M. J.; Alvarenga, J.; Kim, P.; Aizenberg, J. Design of Anti-Icing Surfaces: Smooth, Textured or Slippery? *Nat. Rev. Mater.* **2016**, *1* (1).
(10) Lee, S. J.; Kim, H. N.; Choi, W.; Yoon, G. Y.; Seo, E. A Nature-Inspired Lubricant-Infused Surface for Sustainable Drag Reduction. *Soft Matter* **2019**, *15* (42), 8459–8467.
(11) Preston, D. J.; Lu, Z.; Song, Y.; Zhao, Y.; Wilke, K. L.; Antao, D. S.; Louis, M.; Wang, E. N. Heat Transfer Enhancement during Water and Hydrocarbon Condensation on Lubricant Infused Surfaces. *Sci. Rep.* **2018**, *8* (1), 1–9.
(12) Amini, S.; Kolle, S.; Petrone, L.; Ahanotu, O.; Sunny, S.; Sutanto, C. N.; Hoon, S.; Cohen, L.; Weaver, J. C.; Aizenberg, J.; Vogel, N.; Miserez, A. Preventing Mussel Adhesion Using Lubricant-Infused Materials. *Science* **2017**, *357* (6352), 668–673.
(13) Howell, C.; Grinthal, A.; Sunny, S.; Aizenberg, M.; Aizenberg, J. Designing Liquid-Infused Surfaces for Medical Applications: A Review. *Adv. Mater.* **2018**, *30* (50), 1–26.
(14) Sotiri, I.; Overton, J. C.; Waterhouse, A.; Howell, C. Immobilized Liquid Layers: A New Approach to Anti-Adhesion Surfaces for Medical Applications. *Exp. Biol. Med.* **2016**, *241* (9), 909–918.
(15) Brown, P. S.; Bhushan, B. Liquid-Impregnated Porous Polypropylene Surfaces for Liquid Repellency. *J. Colloid Interface Sci.* **2017**, *487*, 437–443.

(16) Wang, W.; Timonen, J. V. I.; Carlson, A.; Drotlef, D. M.; Zhang, C. T.; Kolle, S.; Grinthal, A.; Wong, T. S.; Hatton, B.; Kang, S. H.; Kennedy, S.; Chi, J.; Blough, R. T.; Sitti, M.; Mahadevan, L.; Aizenberg, J. Multifunctional Ferrofluid-Infused Surfaces with Reconfigurable Multiscale Topography. *Nature* **2018**, *559* (7712), 77–82.
(17) Villegas, M.; Zhang, Y.; Abu Jarad, N.; Soleymani, L.; Didar, T. F. Liquid-Infused Surfaces: A Review of Theory, Design, and Applications. *ACS Nano* **2019**, *13* (8), 8517–8536.
(18) Kreder, M. J.; Daniel, D.; Tetreault, A.; Cao, Z.; Lemaire, B.; Timonen, J. V. I.; Aizenberg, J. Film Dynamics and Lubricant Depletion by Droplets Moving on Lubricated Surfaces. *Phys. Rev. X* **2018**, *8* (3), 031053.
(19) Wexler, J. S.; Jacobi, I.; Stone, H. A. Shear-Driven Failure of Liquid-Infused Surfaces. *Phys. Rev. Lett.* **2015**, *114* (16), 168301.
(20) Michalska, M.; Gambacorta, F.; Divan, R.; Aranson, I. S.; Sokolov, A.; Noirot, P.; Laible, P. D. Tuning Antimicrobial Properties of Biomimetic Nanopatterned Surfaces. *Nanoscale* **2018**, *10* (14), 6639–6650.
(21) Peppou-Chapman, S.; Hong, J. K.; Waterhouse, A.; Neto, C. Life and Death of Liquid-Infused Surfaces: A Review on the Choice, Analysis and Fate of the Infused Liquid Layer. *Chem. Soc. Rev.* **2020**, *49* (11), 3688–3715.
(22) De Gennes, Pierre-Gilles, Françoise Brochard-Wyart, D. Q. *Capillarity and Wetting Phenomena: Drops, Bubbles, Pearls, Waves.*; 2013.
(23) Kim, P.; Kreder, M. J.; Alvarenga, J.; Aizenberg, J. Hierarchical or Not? Effect of the Length Scale and Hierarchy of the Surface Roughness on Omniphobicity of Lubricant-Infused Substrates. *Nano Lett.* **2013**, *13* (4), 1793–1799.
(24) Vogel, N.; Belisle, R. A.; Hatton, B.; Wong, T.-S.; Aizenberg, J. Transparency and Damage Tolerance of Patternable Omniphobic Lubricated Surfaces Based on Inverse Colloidal Monolayers. *Nat. Commun.* **2013**, *4* (1), 2176.
(25) Wong, W. S. Y.; Hegner, K. I.; Donadei, V.; Hauer, L.; Naga, A.; Vollmer, D. Capillary Balancing: Designing Frost-Resistant Lubricant-Infused Surfaces. *Nano Lett.* **2020**, *20* (12), 8508–8515.
(26) Lee, J.; Jiang, Y.; Hizal, F.; Ban, G. H.; Jun, S.; Choi, C. H. Durable Omniphobicity of Oil-Impregnated Anodic Aluminum Oxide Nanostructured Surfaces. *J. Colloid Interface Sci.* **2019**, *553*, 734–745.
(27) Cui, J.; Zhu, H.; Tu, Z.; Niu, D.; Liu, G.; Bei, Y.; Zhu, Q. Effect of the Texture Geometry on the Slippery Behavior of Liquid-Infused Nanoporous Surfaces. *J. Mater. Sci.* **2019**, *54* (3), 2729–2739.
(28) Laney, S. K.; Li, T.; Michalska, M.; Ramirez, F.; Portnoi, M.; Oh, J.; Tiwari, M. K.; Thayne, I. G.; Parkin, I. P.; Papakonstantinou, I. Spacer-Defined Intrinsic Multiple Patterning. *ACS Nano* **2020**, *14* (9), 12091–12100.
(29) Chen, X.; Wen, G.; Guo, Z. What Are the Design Principles, from the Choice of Lubricants and Structures to the Preparation Method, for a Stable Slippery Lubricant-Infused Porous Surface? *Mater. Horizons* **2020**, *7* (7), 1697–1726.
(30) Peng, C.; Chen, Z.; Tiwari, M. K. All-Organic Superhydrophobic Coatings with Mechanochemical Robustness and Liquid Impalement Resistance. *Nat. Mater.* **2018**, *17* (4), 355–360.
(31) Al-Sharafi, A.; Yilbas, B. S.; Hassan, G. Droplet on Oil Impregnated Surface: Temperature and Velocity Fields. *Int. J. Therm. Sci.* **2019**, *146* (August), 106054.
(32) Lee, J.; Jiang, Y.; Hizal, F.; Ban, G.-H.; Jun, S.; Choi, C.-H. Durable Omniphobicity of Oil-Impregnated Anodic Aluminum Oxide Nanostructured Surfaces. *J. Colloid Interface Sci.* **2019**, *553*, 734–745.
(33) Weisensee, P. B.; Wang, Y.; Qian, H.; Schultz, D.; King, W. P.; Miljkovic, N.

Condensate Droplet Size Distribution on Lubricant-Infused Surfaces. *Int. J. Heat Mass Transf.* **2017**, *109*, 187–199.

(34) Sett, S.; Yan, X.; Barac, G.; Bolton, L. W.; Miljkovic, N. Lubricant-Infused Surfaces for Low-Surface-Tension Fluids: Promise versus Reality. *ACS Appl. Mater. Interfaces* **2017**, *9* (41), 36400–36408.

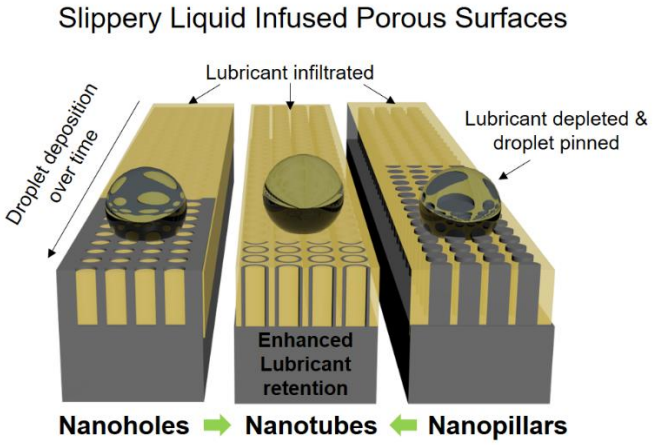

Table of Contents